Efficient simulation of adaptive optics technologies for the Euro50 telescope

Ralf C. Flicker[a] and Patrick C. McGuire[b]

[a]Lund Observatory, Box 43, SE-22100 Lund, Sweden
[b]Center for Astrobiology (INTA/CSIC), Madrid(Torrejon de Ardoz), Spain

ABSTRACT

An efficient adaptive optics (AO) simulation code was developed, which enables first-order simulations of extremely high-order systems. The Monte-Carlo-type code employs a sparse conjugate gradient algorithm for wavefront reconstruction, and a separation of spatial frequencies into two domains to economize on the number crunching. High-order multi-conjugate adaptive optics (MCAO) systems are thereby readily simulated on a single standard PC. The code is presently being applied to MCAO design studies for the Euro50 extremely large telescope (ELT), addressing a number of issues not previously subjected to realistic simulation due to the excessive computational load. We report in this paper on the latest results obtained from simulating two specific aspects of the Euro50 AO system: turbulence prediction and laser guide star (LGS) beacon synthesis. The two studies presented here are representative examples of a number of technology studies being enabled by the new fast simulation codes.

1. INTRODUCTION

It was recognized in recent years that new simulation methods had to be developed in order to efficiently study very-high-order AO and MCAO systems.[1] The advent of a number of ELT projects have created a need for detailed simulations of MCAO systems incorporating multiple deformable mirrors (DMs) with $O(10^4)$ actuators and multiple reference beacons producing $O(10^5)$ wavefront sensor (WFS) outputs. The bottleneck in scaling up existing adaptive optics simulation codes to these dimensions turned out to be the process of wavefront reconstruction, which in it's traditional linear implementation is carried out by a single matrix-vector multiplication per real-time frame. The complexity of that computation is $2mn$ floating-point operations, where m and n are the dimensions of the reconstruction matrix (total number of WFS outputs and DM actuators, respectively). Assuming for simplicity $O(m) = O(n)$ (usually true), the computational complexity scales as $O(n^2)$. Since $n \propto D^2$, with D being the telescope diameter, the resultant scaling $O(D^4)$ signals a potential real-time control problem as the telescope becomes very large, and furthermore the matrix inversion required to compute the reconstructor is of complexity $O(D^6)$. At kHz frame rates, the required real-time computing power is thereby in some extreme cases pushed into the TFlops range, which seems not to be a viable solution for the foreseeable future.

While there are several candidates for more efficient algorithms, this paper shall be concerned solely with methods that take advantage of the sparseness of the adaptive optics system matrix. The reader may consult the references for, e.g., Fourier domain methods that do wavefront reconstruction at FFT speeds.[2] Although sparse matrix technologies were applied to wavefront reconstruction of conventional AO systems already at an early stage,[3] it is only recently that the concept was developed for MCAO and applied to the problem of ELT simulation.[4] At the present, a number of efficient estimation algorithms have been devised and tested, which achieve efficiencies ranging around $O(n^{3/2})$ to $O(n \log n)$ and approaching in some cases $O(n)$.[2–6] The adaptive optics simulations presented in this paper were produced by the code described in Flicker (2003).[6] Therefore only a brief summary of the method will be given here, in Section 2, and the emphasis of the paper lies instead on the applications.

Euro50 is a European consortium carrying out feasibility studies and initial design studies of a 50-m optical telescope, which is to be equipped with a LGS-based MCAO system deeply integrated into the telescope design. The studies undertaken so far are presented in the Euro50 "white book".[7] The current investigation has focused on the amelioration of two types of adaptive optics wavefront errors: the focal anisoplanatism associated with laser guide stars at a finite range, and the time delay error resulting from the finite temporal bandwidth and additional latency

Further author information (send correspondence to R.C.F.):
E-mail: ralf@astro.lu.se (R.C.F.); mcguire@inta.es (P.C.M.)

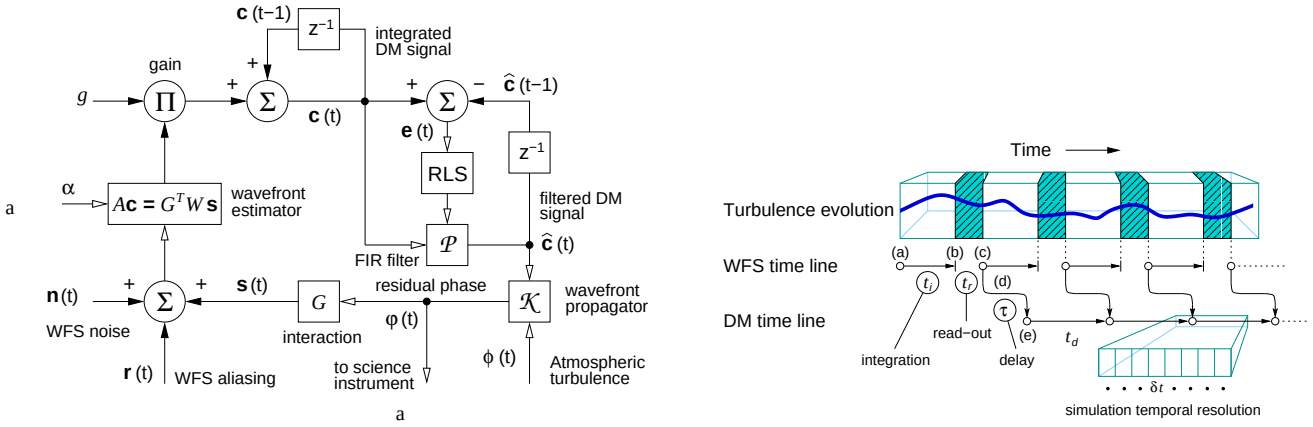

Figure 1. Left—block diagram of the simulation code, including the RLS predictor. Right—schematic of the temporal sequencing implemented in the simulation, indicating the tunable temporal oversampling. Symbols and variables are explained in the text.

in the control loop. While well understood at more moderate scales, their manifestations in a system designed for a 50-m telescope have not previously been subjected to realistic simulation, due to the excessive computational load and a lack of efficient simulation codes. The two technologies to be investigated here for the mitigation of these errors are, respectively, a LGS beacon synthesis approach and neural network temporal turbulence prediction, as described in Sections 3 and 4.

2. FIRST-ORDER ELT SIMULATION

A block diagram of the simulation code and it's temporal sequencing is shown in Fig. 1. Of it's main features and limitations, the most important are:

- maximum a posteriori (MAP) tomographic wavefront reconstruction implemented by a sparse preconditioned conjugate gradient (PCG) solver
- dichotomy of spatial frequencies: simulating only LF component and estimating HF errors by separate simulation codes or analytical models of the asymptotic long-exposure result
- linear wavefront propagation - scintillation can not be modeled
- separate LGS-MCAO null-mode compensation
- enhanced and tunable temporal resolution
- predictive control and LGS beacon synthesis

The predictor to be investigated in Section 4 is represented by the recursive least-squares (RLS) box and the linear filter $\mathcal{P}$, and the z^{-1} boxes represent unit frame delays. The temporal sequencing diagram merely serves to illustrate the tunable temporal resolution δt, which enables the simulation to capture realistically the temporal dynamics and stability properties of the adaptive optics system.

2.1. Efficient wavefront estimation

The wavefront estimator is of the standard open loop MAP type, employing Ellerbroek's approximation[4] to render the regularization term C^TC sparse. Assuming identical reference beacons, the linear system to be solved for the actuator adjustment vector $\mathbf{c}$ is

$$\underbrace{(G^TG + \alpha C^TC)}_{A}\,\mathbf{c} = G^T\mathbf{s} = \mathbf{b}, \tag{1}$$

where G is the DM-to-WFS interaction matrix, $\mathbf{s}$ is the vector of WFS signals, C a discrete representation of the Laplacian (curvature) operator ∇^2 and α a scalar parameter determining the influence of the regularization term.

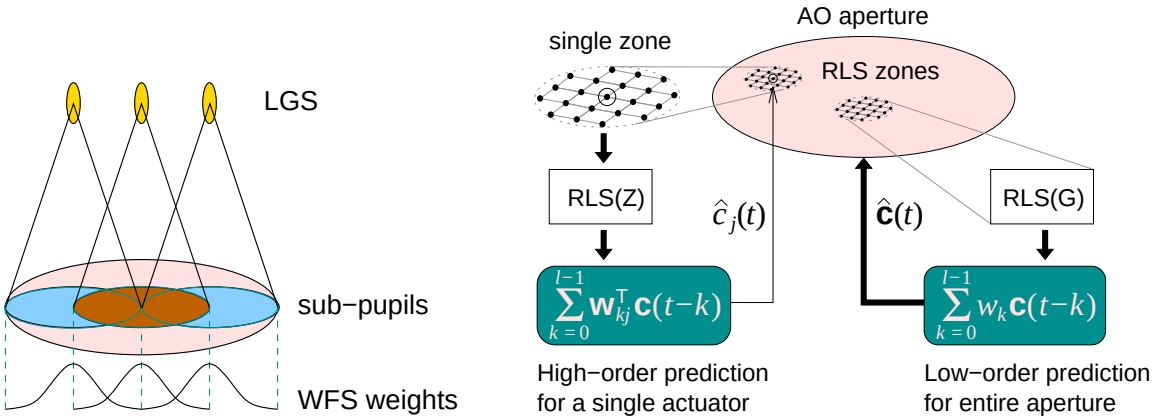

Figure 2. Left—schematic of LGS beacon synthesis by WFS sub-aperture weights, as discussed in Section 3. Right—illustration of the global and zonal prediction schemes discussed in Section 4.

The approximation $\langle \mathbf{c}\mathbf{c}^T \rangle^{-1} \approx C^T C$ relies upon applying the Kolmogorov model to the spatial statistics of $\mathbf{c}$, and approximating the Kolmogorov power law by $\kappa^{-11/3} \approx \kappa^{-4}$, where κ is the spatial frequency. It is interesting to note that the bi-harmonic term which emerges upon this approximation is a special case of the penalty term in the Tikhonov functional. The matrix C has at most five elements per column, which makes $C^T C$ very sparse for large systems. The vector $\mathbf{b}$ is computed by a sparse matrix-vector multiplication, and the resultant system $A\mathbf{c} = \mathbf{b}$ is then solved by PCG iterations. A simple Jacobi preconditioner was used in this case. The closed loop instabilities that appear to be a problem with the sparse implementation of the minimum variance estimator[8] are not observed with this MAP estimator and the current code.

3. LASER BEACON SYNTHESIS

To introduce a minimum of Euro50 terminology, it is desired that the telescope is able to offer (among other things): a single-conjugate adaptive optics (SCAO) mode using only one DM but multiple LGSs, and a dual-conjugate adaptive optics (DCAO) mode using two DMs and multiple LGSs. In SCAO the DM is conjugated close to the telescope pupil, and the purpose is to have a mode of partial adaptive correction with superior optical throughput. A wide-field "seeing-improved" mode of SCAO is currently under consideration, but the topic of interest here is the opposite, the zero-field SCAO application where one uses multiple LGSs to achieve the best possible correction on the optical axis.

3.1. Focal anisoplanatism in SCAO

For Kolmogorov turbulence, the mean square phase error due to the cone effect on a single beam scales as $D^{5/3}$ (Fried & Belsher, 1994).[9] This means a 20-fold increase in the mean-square phase error in going from an 8-m telescope to a 50-m telescope, which would result in an on-axis K band (2.2 μm) Strehl ratio of only $\sim 0.1 - 0.15$ for the Euro50. The use of multiple LGSs and tomography, however, in combination with the finite outer scale of atmospheric turbulence completely fudges this simple scaling law, which is why rigorous simulations are required for ELT-class MCAO systems in order to be able to answer such perceptive questions as "how many LGSs do we need?"

Using multiple LGSs in DCAO mode, the distortion of the WFS signal induced by the LGS beam magnification is canceled in the wavefront reconstruction process, by virtue of this magnification being calibrated into the interaction matrix G. This is the essence of tomography and least-square-error projection onto DMs done in a single step. Whether this is the best way to do it remains debated, and while several alternative methods have been proposed, none, to the best of the authors' knowledge, has convincingly demonstrated superior performance.

In SCAO mode, the cone effect can not be calibrated into the system by measuring it, so left to its own devices the system is unable to cancel the cone effect. Applying a standard least-squares estimator anyway only amounts to averaging the signal from all the LGS beams, with a very poor result. Two approaches to ameliorate the cone effect in this case are to either prevent the error from arising in the first place by the beacon synthesis method to be investigated in the following, or to attempt tomography in SCAO. The latter could be implemented either by an explicit tomography step followed by a linear projection or, it has been proposed, by Fourier-domain-based

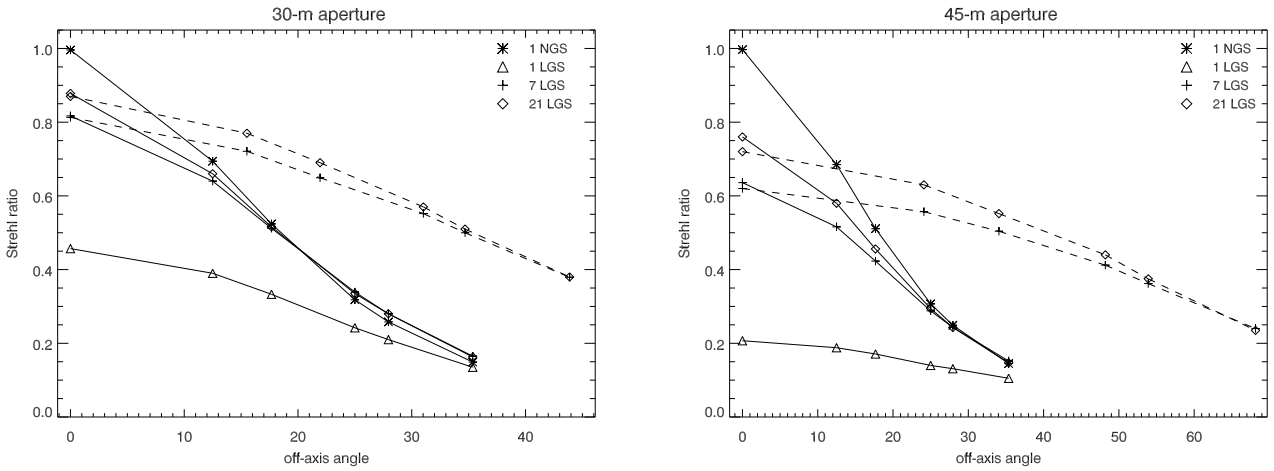

Figure 3. Anisoplanatism Strehl ratios for SCAO LGS beacon synthesis at 2.2 μm over 30-m and 45-m apertures, with 7 (pluses) and 21 (diamonds) LGSs. For reference, the case of a single NGS (asterisks) and a single LGS (triangles) are shown, and for comparison also the zero-FoV DCAO case (dashed lines).

back-projection algorithms. It is the opinion of the authors that a standard tomography step holds the promise of best performance per number of guide stars, but awaiting those simulation results it is the beacon synthesis results that are presented here.

The LGS beacon synthesis solution proposed for the Euro50[10] is illustrated in Fig. 2. By weighing the LGS signals appropriately, one artificially reduces the base of each cone over the WFS pupil. Thus, by virtue of not making full-aperture measurements, each signal is less corrupted by the cone effect, and by a linear combination (Hanning windows) the LGSs together "synthesize" a single collimated full-aperture beam. It must be noted that there was no additional stitching algorithm applied here to phase the beams. The full-aperture tilt was removed from each of the beams, which normally would cause the Hanning-shaped beams to be joined together with erroneous sub-pupil tilts. We have not solved this problem, but we observe that in the current setting the stitching error appears to be small ("appears" because we do not have a correctly stitched reference to compare with). The reason for this we believe to be the relatively high-bandwidth closed loop tip/tilt correction, and the outer scale of the turbulence (50 m in these simulations). The tilt is almost perfectly corrected, and since it changes relatively slowly over the large aperture and is furthermore attenuated and broken up by the outer scale, the LGSs see very little tip/tilt. The stitching error can therefore be small enough that performance is not prohibitively degraded by it.

The simulation results are shown in Fig. 3, which addresses only the focal anisoplanatism (i.e. no other AO related errors). It is clear that, using the beacon synthesis method, it will be hard to push the focal anisoplanatism Strehl ratio beyond 0.8 even in K band for the Euro50. For the two configurations simulated, using 21 and 7 LGSs, on-axis Strehl ratios of 0.72 and 0.62 were obtained. For comparison, the same numbers for a 30-m aperture comes out to 0.87 and 0.81. It was also found that increasing the number of LGSs to 37 brought only a marginal improvement, which implies that it could become exceedingly expensive in terms of LGSs to push the Strehl ratio beyond the current simulation values, using the synthesis method.

4. TEMPORAL TURBULENCE PREDICTION

The rationale for implementing a prediction step in the control of an adaptive optics system is to reduce the servo-lag error. Prediction may be applied either to the WFS signal, whereby it acts as a preprocessor to the wavefront reconstructor, or to the DM signal itself. While artificial neural networks offer a general means for adaptive, nonlinear function approximation,[11] it was found by McGuire et al. (2000)[12] that a linear network trained with a recursive least-squares (RLS) algorithm could combine rapid convergence with excellent prediction performance. This forms the basis for the current investigation, but the predictor is here implemented as an adaptive linear filter acting on the DM signal, as indicated in Fig. 1. Our goal will be to test various prediction implementations on an AO system of the scope that the Euro50 SCAO mode represents ($\sim$ 3000 actuators).

4.1. Regression models

The RLS algorithm may be applied in various implementations depending upon the formulation of the regression model representing the system. Adopting the notation of Strobach (1990),[13] the regression variable $x(t)$ may be formulated according to an *ensemble* definition or a *time* definition:

$$\text{ensemble definition :} \quad \mathbf{x}_e(t) = [x_0(t), x_1(t), \ldots, x_{m-1}(t)]^T, \tag{2}$$

$$\text{time definition :} \quad \mathbf{x}_t(t) = [x(t), x(t-1), \ldots, x(t-n+1)]^T, \tag{3}$$

or combining both on a vector or matrix form:

$$\text{vector form :} \quad \mathbf{x}(t) = [\mathbf{x}_e^T(t), \mathbf{x}_e^T(t-1), \ldots, \mathbf{x}_e^T(t-n+1)]^T, \tag{4}$$

$$\text{matrix form :} \quad X(t) = [\mathbf{x}_e(t), \mathbf{x}_e(t-1), \ldots, \mathbf{x}_e(t-n+1)]^T. \tag{5}$$

If $\mathbf{y}(t) = \mathbf{x}_e(t)$ is the vector of observed variables and $\widehat{\mathbf{y}}(t)$ the prediction, two possible regression models are:

$$\widehat{\mathbf{y}}(t) = W\mathbf{x}(t), \tag{6}$$

$$\widehat{\mathbf{y}}(t) = X^T(t)\mathbf{w}, \tag{7}$$

where $\mathbf{w}$ is the column vector of model parameters (i.e. the synaptic weights in a neural network description) and W a row matrix composed of the vectors $\mathbf{w}_j^T$ corresponding to the individual elements $\widehat{y}_j$ of the output vector. While the first form allows for a unique set of weights for each variable $\widehat{y}_j$, the second form leads to all the elements of $\widehat{\mathbf{y}}$ sharing the same set of weights. Henceforth the model (6) will be referred to as the *zonal* predictor, and the model (7) as the *global* predictor. These are illustrated schematically in Fig. 2. The least-squares inverse problem consists of finding the weights W that minimize $\|\widehat{\mathbf{y}} - \mathbf{y}\|_2$. The RLS algorithm proceeds to do this by the recursive updating of both W and P, the inverse covariance matrix of X. As an intermediate computational step there also appears the Kalman gain vector K. The dimensions of these (P, W, K) depend upon the number of look-backs n and the number of adaptive elements m, and which regression model is used. In its most compact form, the standard formulation of the RLS algorithm with exponential forgetting (the λ factor) is[14]

$$K(t) = P(t-1)x(t)[\lambda I + x^T(t)P(t-1)x(t)]^{-1} \tag{8}$$

$$P(t) = \lambda^{-1}[I - K(t)x^T(t)]P(t-1) \tag{9}$$

$$w(t) = w(t-1) + K(t)[y(t) - x^T(t)w(t-1)], \tag{10}$$

where the boldface/matrix notation for the regression variables and the weights were dropped, as their dimensions depend upon the choice of regression model.

4.2. Zonal prediction

The zonal approach based on the vector form (4) and the regression model (6) enables an abundance of degrees of freedom, but the updating of the inverse covariance matrix P becomes an increasingly ill-conditioned problem as its dimensions grow. One way to improve numerical behavior of the RLS is via Kubin's "selective memory" algorithm, which is based upon Potter's square-root factorization $P = Q^TQ$. The algorithm, which involves only scalar divisions, entails the following computations, where for clarity the dimensions of the quantities are listed in the left column:[13]

$$\mathcal{R}^{mn\times 1} \quad \mathbf{x}'(t) = Q(t-1)\mathbf{x}(t) \tag{11}$$

$$\mathcal{R}^{mn\times 1} \quad \mathbf{k}(t) = Q^T(t-1)\mathbf{x}'(t) \tag{12}$$

$$\mathcal{R}^{1} \quad \alpha(t) = \lambda + \|\mathbf{x}'(t)\|^2 \tag{13}$$

$$\mathcal{R}^{1} \quad \beta(t) = (\alpha^{-1/2}(t) - 1)(\alpha(t) - \lambda)^{-1} \tag{14}$$

$$\mathcal{R}^{mn\times mn} \quad Q(t) = Q(t-1) + \mathbf{x}'(t)\mathbf{k}^T(t)\beta(t)/\alpha(t) \tag{15}$$

$$\mathcal{R}^{m\times 1} \quad \mathbf{e}(t) = \mathbf{y}(t) - W(t-1)\mathbf{x}(t) \tag{16}$$

$$\mathcal{R}^{m\times mn} \quad W(t) = W(t-1) + \mathbf{e}(t)\mathbf{k}^T(t)/\alpha(t). \tag{17}$$

The sequence (11)-(17) updates W and Q for a recursion zone of size m. In the current prediction scheme, a zone is centered on each actuator (except for the edge actuators). The prediction for the entire ensemble is then formed as a linear combination of predictions produced by all the overlapping zones.

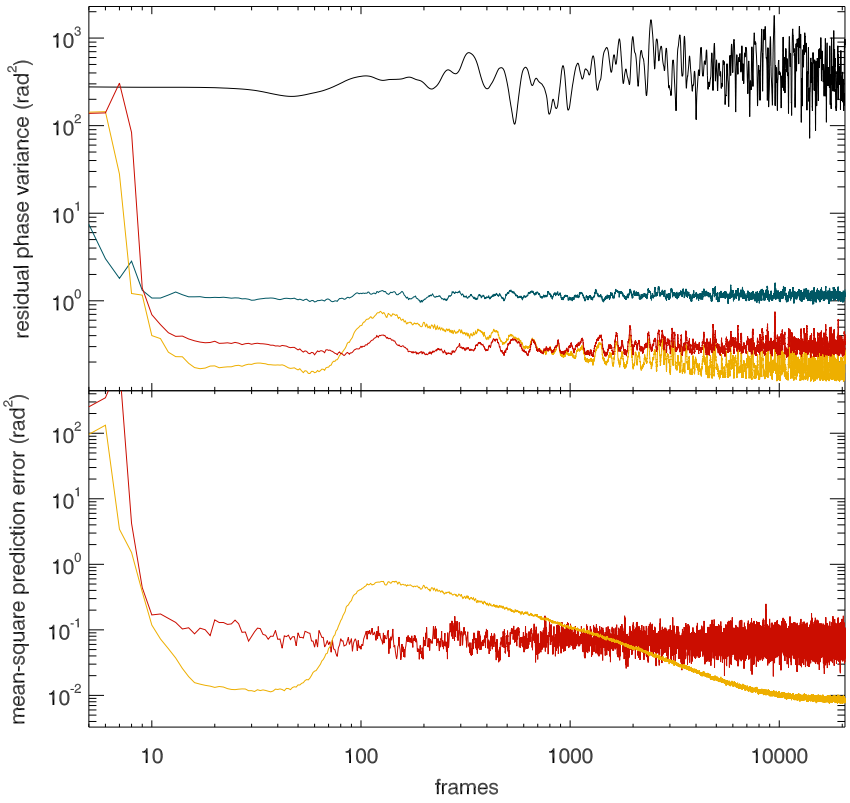

Figure 4. V band ($\lambda = 0.5$ μm, $r_0 = 0.1$ m) SCAO for $D = 50$ m and 3000 actuators: off-line prediction with the zonal (yellow) and global (red) predictors at a look-back of $n = 5$ (blue = no prediction; black = no AO). The top part shows the residual mean-square phase error on the corrected beam, while the lower part shows the mean-square of the error signal $\mathbf{e}(t)$, which indicates the magnitude of the adjustment applied in the RLS algorithm.

4.3. Global prediction

Assuming the matrix form (5) and the regression model (7) results in an implementation of the RLS which has some interesting properties. The algorithm, which involves a $m \times m$ matrix inversion, may be broken down into the following computations:

$$\begin{aligned}
\mathcal{R}^{n\times m} \quad k(t) &= P(t-1)X(t) && (18)\\
\mathcal{R}^{m\times m} \quad \alpha(t) &= \lambda I + X^T(t)k(t) && (19)\\
\mathcal{R}^{n\times m} \quad K(t) &= k(t)\alpha^{-1}(t) && (20)\\
\mathcal{R}^{n\times n} \quad P(t) &= \lambda^{-1}[P(t-1) - K(t)k^T(t)] && (21)\\
\mathcal{R}^{m\times 1} \quad \mathbf{e}(t) &= \mathbf{y}(t) - X^T(t)\mathbf{w}(t-1) && (22)\\
\mathcal{R}^{n\times 1} \quad \mathbf{w}(t) &= \mathbf{w}(t-1) + K(t)\mathbf{e}(t). && (23)
\end{aligned}$$

The symmetry of P was used on line (21). Apart from having fewer degrees of freedom (by orders of magnitude) than the zonal predictor, the distribution and flow of spatial and temporal information is also very different. In Kubin's algorithm, the scalar α parameter acts only as a normalization factor. In the algorithm above, the dimensions of Q and α suggest that spatial information has been shifted from P to α, which is inverted at (20). This explicit matrix inversion is presumably why the algorithm, despite its few free parameters, exhibits quite good performance and extremely fast convergence.

4.4. Cost analysis

The computational complexity of the algorithms impinge upon the number crunching and storage capacities required to implement the predictors. The global predictor has only n filter weights to update regardless of the size of the

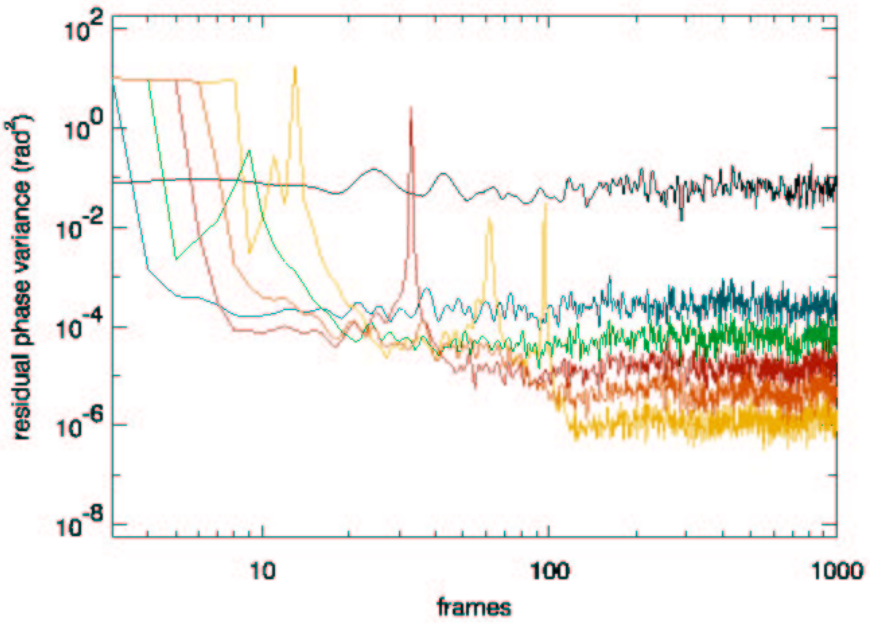

Figure 5. Online closed loop prediction with the global predictor, for a range of look-backs: $n = 3, 4, 5, 6, 8$ blue→yellow (black = no prediction). $D = 8$ m, 3000 actuators, $\lambda = 1$ μm.

system, and the most demanding step in the algorithm is the $m \times m$ matrix inversion. A zone of 4×4 actuators (i.e. $m = 16$) centered on the DM was the default setting for the global predictor. Increasing the size of the zone will quickly lead to demanding matrix inversions that ultimately can not be carried out in real time. Including the entire aperture in the recursion zone would require a $N \times N$ matrix inversion, where N is the number of actuators, which is an $O(N^3)$ process. Apart from the computational penalty for large N, the benefit of using a large zone with the global predictor is limited, since the filter ultimately has no spatial degrees of freedom to account for statistical variations across the pupil.

The zonal predictor requires the computation and storage of a $N \times m \times mn$ filter weight cube and a $N \times mn \times mn$ Q-cube, which are of complexities $O(Nm^2n)$ and $O(Nm^2n^2)$. While the linear scaling with N is benign for very large systems, the quadratic scaling with m makes it clear that a recursion zone can not extend very far before storage becomes expensive and convergence too slow. Luckily, for adaptive optics turbulence prediction, the spatial and temporal correlations for a small number of look-backs are for the most part local. Zones with 3×3 or 4×4 spatial elements are usually able to capture most of the relevant statistics. While this still leads to pretty big Q matrices if the system is large, it should be contrasted to the case of a full-aperture zone. In this case we find W- and Q-complexities of $O(N^2n)$ and $O(N^2n^2)$, where the quadratic scaling with N immediately spells trouble for very large systems. The gain in efficiency with the zonal predictor scales as N/m^2, which means that the zonal predictor becomes more efficient than a full-aperture predictor as soon as $N > m^2$.

4.5. Sample numerical results

Figures 4 and 5 show two sample simulation results for a conventional AO system with 3000 actuators. In Fig. 4 the setting is off-line global/zonal prediction over a 50-m aperture at $\lambda = 0.5$ μm with a look-back of $n = 5$, and in Fig. 5 we test the global predictor in online closed loop on a 8-m aperture at $\lambda = 1$ μm for a range of look-backs. It is noteworthy that a very efficient simulation was required to obtain these results—simulating 20 000 frames would not be feasible if a single frame took more than a few minutes. The global predictor is invariably seen to converge within 10-100 frames, depending upon the number of look-back steps, while the zonal predictor in the first case requires $O(10^4)$ frames to reach the minimum error level. The prominent feature of the zonal predictor error in Fig. 4 is the fast initial drop, followed by a sharp rise and then a much slower convergence to the final level. We interpret this as the predictor rapidly adjusting to the initial conditions, and as the turbulence evolves away from this state the predictor begins the process of learning the spatial-temporal statistics. For a beast of 1.2×10^6 degrees of freedom, the zonal predictor still converges reasonably fast—it outperforms the global predictor with its modest 5

degrees of freedom after only 1000 frames, and is close to its minimum after 10^4 frames. Measured in Strehl ratios, the performance of the zonal predictor after 20 000 frames (50-m case, V band) was 0.88, noting 0.77 for the global predictor and 0.26 for the AO system without any prediction at all.

5. CONCLUSIONS

By the use of efficient wavefront estimation algorithms based upon sparse matrix techniques, it is possible to simulate very-high-order adaptive optics systems such as are foreseen for the extremely large telescopes of the future. Using such an efficient simulation code, investigations into laser guide star beacon synthesis and temporal turbulence prediction were undertaken for the Euro50 adaptive optics system. The method of LGS synthesis was shown to be able to deliver appreciable on-axis performance, however at the expense of a large number of LGSs. It is believed that a single-conjugate tomography algorithm will be able to do better, and this is being investigated currently. The tests of two different temporal turbulence predictors revealed that the low-order global predictor converges extremely fast and remains stable even in online closed loop prediction. The high-order zonal predictor offers superior performance, however at the expense of much slower training, and online prediction stability could not be demonstrated. Future work will continue to investigate the properties of these predictors and develop modified algorithms to improve online stability, noise robustness and computational efficiency.

REFERENCES

1. B. L. Ellerbroek and F. J. Rigaut, "Scaling Multi-Conjugate Adaptive Optics Performance Estimates to Extremely Large Telescopes," in *Adaptive Optical Systems Technology*, vol. 4007 of *Proc. SPIE*, march 2000.
2. L. A. Poyneer, D. T. Gavel, and J. M. Brase, "Fast wave-front reconstruction in large adaptive optics systems with use of the Fourier transform," *J. Opt. Soc. Am. A* **19**, pp. 2100–2111, October 2002.
3. G. M. Cochran, "Sparse matrix techniques in wavefront reconstruction," Tech. Rep. No. TR-668, The Optical Sciences Company, Anaheim, CA-92825, USA, 1986.
4. B. L. Ellerbroek, "Efficient computation of minimum-variance wave-front reconstructors with sparse matrix techniques," *J. Opt. Soc. Am. A* **19**, pp. 1803–1816, September 2002.
5. L. Gilles, C. R. Vogel, and B. L. Ellerbroek, "Multigrid preconditioned conjugate-gradient method for large-scale wave-front reconstruction," *J. Opt. Soc. Am. A* **19**, pp. 1817–1822, September 2002.
6. R. C. Flicker, "Efficient first-order performance estimation for high-order adaptive optics systems," *Astron. Astrophys.* **405**, pp. 1177–1189, July 2003.
7. T. Andersen, A. Ardeberg, and M. Owner-Petersen, eds., *Euro50: A 50 m Adaptive Optics Telescope*, Lund Observatory, Lund, Sweden, 2003.
8. B. L. Ellerbroek and C. R. Vogel, "Simulations of closed-loop wavefront reconstruction for multi-conjugate adaptive optics on giant telescopes," in *Astronomical Adaptive Optics Systems and Applications*, R. K. Tyson and M. Lloyd-Hart, eds., vol. 5169 of *Proc. SPIE*, 2003.
9. D. L. Fried and J. F. Belsher, "Analysis of fundamental limits to artificial-guide-star adaptive-optics-system performance for astronomical imaging," *J. Opt. Soc. Am. A* **11**, pp. 277–287, Jan. 1994.
10. M. Owner-Petersen, T. Andersen, A. V. Goncharov, and J. M. Beckers, "Control strategy for the adaptive optics of the Euro50," in *Future Giant Telescopes. Edited by Angel, J. Roger P.; Gilmozzi, Roberto. Proceedings of the SPIE, Volume 4840, pp. 427-435 (2003).*, pp. 427–435, Jan. 2003.
11. S. Haykin, *Neural Networks: A Comprehensive Foundation*, Prentice-Hall, Inc., 1999.
12. P. C. McGuire, T. A. Rhoadarmer, H. Coy, R. P. Angel, and M. Lloyd-Hart, "Linear zonal atmospheric prediction for adaptive optics," in *Adaptive Optical Systems Technology*, vol. 4007 of *Proc. SPIE*, pp. 682–691, March 2000.
13. P. Strobach, *Linear Prediction Theory: A Mathematical Basis for Adaptive Systems*, Springer Series in Information Sciences, Springer-Verlag, 1990.
14. K. J. Åström and B. Wittenmark, *Adaptive Control*, Addison-Wesley Publishing Company, second ed., 1995.